Specific Features of Content Dependences for Energy Gap in $In_xTl_{1-x}I$ Solid State Crystalline Alloys

A.I. Kashuba[a], M. Piasecki[b], O.V. Bovgyra[a], V.Yo. Stadnyk[a], P. Demchenko[c], A. Fedorchuk[d], A.V. Franiv[a] and B. Andriyevsky[e,*]

[a]Physics Faculty, Ivan Franko National University of Lviv, Kyrylo and Mephodiy str. 8a, Lviv, 79005, Ukraine
[b]Institute of Physics, Jan Długosz University Częstochowa, Armii Krajowej 13/15, Częstochowa, Poland
[c]Department of Inorganic Chemistry, Ivan Franko National University of Lviv, Kyryla and Mephodiy Str. 6, Lviv, 79005, Ukraine
[d]Department of Inorganic and Organic Chemistry, Lviv National University of Veterinary Medicine and Biotechnologies, Pekarska Str. 50, 79010 Lviv, Ukraine
[e]Faculty of Electronics and Computer Sciences, Koszalin University of Technology, Śniadeckich 2, PL-75453, Koszalin, Poland

(Received September 24, 2017; in final form November 15, 2017)

A series of $In_xTl_{1-x}I$ ($x = 0.4-0.9$) single crystalline solid state alloys were successfully synthesized by the vertical Bridgman method. For the first time the density functional theory based band structure calculations are performed and features of the band energy dispersion are discussed. Comparison with the experimental energy gap E_g obtained from the optical photoconductivity is discussed. An essential role of the localized defects and excitons in formation of the edge photoconductivity is analyzed. Relation between the crystal structure and photoconductivity of the materials studied is discussed. Also the origin of the principal valence and conduction bands is explored. Experimental measurements of the band gap E_g by the optical and photoconductivity methods have given opposite dependences with respect to the indium content x. Features of the photoconductivity spectra for different crystallographic directions have been discussed with taking into account the chemical bonds anisotropy.

DOI: 10.12693/APhysPolA.133.68

PACS/topics: 71.20.Nr, 71.20.–b, 42.70.Gi, 71.35.–y

1. Introduction

Single crystals of heavy metal halogenides like TlBr–TlI and TlCl–TlBr are of interest for applications in infrared optics, whereas TlCl and TlCl–TlBr are used in the Cherenkov-light detector radiators [1, 2]. A better opportunity to manage in wide energy range the band gap E_g for practical applications exists with varying the cationic content of InI–TlI (from $E_g = 2.01$ eV for InI to $E_g = 2.9$ eV for TlI). The latter content InI–TlI is also perspective for applications in the wide spectral range — from visible to IR regions.

The titled compounds may be considered as a particular class of binary semiconducting compounds possessing promising optical parameters. For example, there is observed an enhanced attention to the study of physical properties of the crystalline semiconductor compounds $A^{III}B^{VII}$, including binary layered crystals [3, 4]. The traditional crystals with heavy cations, like TlI and Tl–In–I [5, 6], may serve as the suitable modeling crystals and as those for the search and design of novel crystals. Following Ref. [7] they possess a rare coexistence of the ionic and covalence chemical bonds which define a huge anisotropy of the effective masses and carrier mobility. Following these reason one can expect that growth of the corresponding solid crystalline state alloys may be perspective for the design of principally new materials with coexistence the long-range-ordered and locally disordered structures. This fact is also responsible for their very promising photo-induced features [8] and defect-induced phase transitions [9].

In Ref. [10], the band structure calculations of the single crystal InI were performed using the norm-conserving pseudopotential approach and it was concluded that the energy band gap $E_g^{(i)}$ corresponds to the indirect optical transitions. The calculated difference between direct and indirect energy gaps was equal to only $E_g^{(d)} - E_g^{(i)} = 0.04$ eV. This magnitude does not allow to conclude definitively about the nature and place of optical transition localization responsible for the formation of the optical absorption edge.

One of the first *ab initio* studies of the point defects in the crystal InI, using the Vanderbilt ultrasoft pseudopotentials and exchange-correlation potential within a framework of the Perdew–Burke–Ernzerhof (PBE) parametrization and the generalized gradient approximation (GGA), are presented in Ref. [11]. In this study, a band structure for perfect crystal InI is provided, whereby the smallest direct energy gap $E_g^{(d)}$ is localized at the point Γ of the Brillouin zone (BZ). However, in the other studies [10, 12–15], the location of direct energy gap was detected not at Γ point of BZ.

*corresponding author; e-mail: bohdan.andriyevskyy@tu.koszalin.pl

In Ref. [16], the electronic structure of $In_xTl_{l-x}I$ was calculated using the band structure technique described in Refs. [10, 12] within the framework of the local density approximation (LDA). The principal BZ dispersion was theoretically calculated by the linear interpolation between the lattice parameters for the extreme binary compounds according to the Vegard rule. In paper [16], the band structure calculations for three values of concentration x (0.25, 0.5, and 0.75), excluding the extreme binary compounds InI and TlI, were explored at $1\times1\times1$ supercell.

In paper [17], authors calculated the energy band structure of $In_xT_{l-x}I$ using the technique described in [11], i.e. the superlattice $2\times1\times2$ constructed from primitive cells of the orthorhombic lattice symmetry *Cmcm* (63). It was stated in article [17] that the smallest energy gap is localized at the point Q of the BZ.

Comparison of the above mentioned studies reveals their disagreement in the interpretation of band diagrams for both InI and $In_xT_{l-x}I$, prevailingly relating the smallest direct band gap location in the space of the electron wave vector $\boldsymbol{K}$. Therefore, with the purpose of removal of the noted inconsistencies and clarification of $In_xT_{l-x}I$ electronic spectrum peculiarities, we present results of the density functional theory (DFT) calculations using the technique applied in Refs. [11, 16] (ultrasoft Vanderbilt pseudopotentials and exchange-correlation GGA potential).

Contrary to the previous our paper [16], in the present study, we have used the experimental lattice parameters of $In_xT_{l-x}I$ for the calculations of band structure and related values. Earlier studies of InI_xBr_{1-x}, TlI_xBr_{1-x} [18–20] were devoted prevailingly to the anionic substitutions and solid solutions based on them. As a continuation of previous investigations, in the present work, we perform DFT study of the cationic substituted binary compounds $In_xTl_{1-x}I$ and latter we compare the results obtained with our measurements of photoconductivity.

2. Crystal structure

Binary, isostructural TlI and InI crystallize in orthorhombic space group D_{2h}^{17}(*Cmcm* (63)). The structures of both compounds are sandwich layered with two type layers in unit cell and four formula units in it. The layers are oriented perpendicular to the crystallographic b-axis. Lattice parameters depend on the composition of the solid solution [21]. In layers, at different location the I–I bonds are slightly reduced with respect to the bond length corresponding to ionic radii (ion radius of I is 2.20 Å). Based on the nature and location of the reduced distances (Fig. 1) the stratification is more pronounced for TlI. Within the layers it can be identified mainly by the iodine atoms along the crystallographic direction [001] (Fig. 1).

As we will show later, a continuous variation of the lattice parameters in the absence of structural phase transitions is observed. It should be noticed that a substitution Br by I in the anion sublattice of InI_xBr_{1-x} and TlI_xBr_{1-x} changes the corresponding energy gaps $E_g(x)$ slightly (0.05–0.1 eV) ($x = 0.01-0.1$) in comparison to the much larger difference of E_g corresponding to the change in the cation subsystem, $E_g = 2.01$ eV for InI, and $E_g = 2.9$ eV for TlI [22, 23]. Studies of the optical properties near the fundamental absorption edge for $In_xTl_{1-x}I$ give opportunity to determine the nature of the physical mechanisms involving appearance of the localized defects and excitonic resonances. According to Ref. [24], such studies were carried out for a and c crystallographic directions for several compositions of $In_xTl_{1-x}I$. Along these directions, one can find the corrugated chains of metal atoms. As it seen in Fig. 2, one can also expect a formation of the non-zero ground state dipole moment.

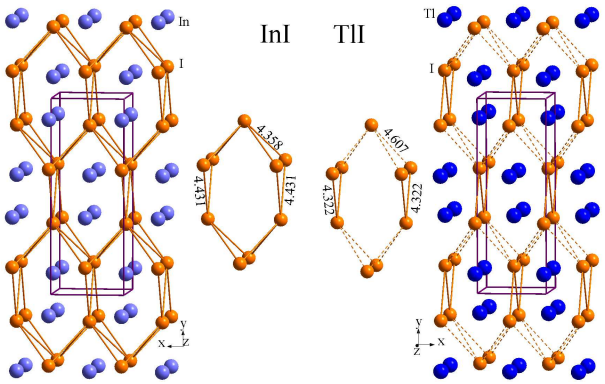

Fig. 1. Principal chemical bond distances I–I (orange, in Å) in the structure of compounds InI and TlI.

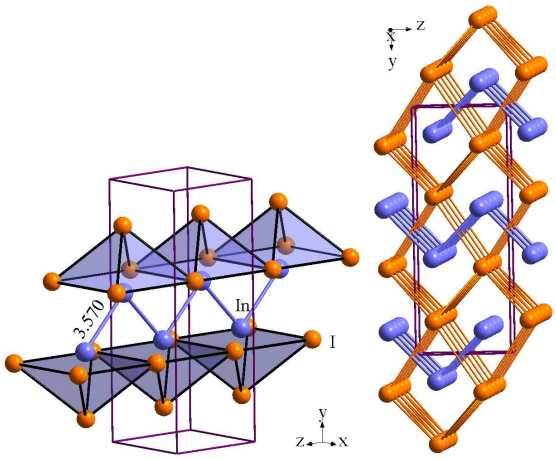

Fig. 2. Presentation of corrugated metal chains for principal atoms in the structure of TlI or InI crystals.

One can also expect an increase of the number of defects along with the x-associated deviations from the perfect compounds InI and TlI.

The main goal of the present study is a study of variations of the optical constants for homogeneous, high quality $In_xTl_{1-x}I$ solid state crystalline alloys obtained using the Bridgman–Stockbarger technique in the wide range of Tl concentration ($x = 0.3-0.9$). We have performed detailed investigations of the crystalline structure

along with the analysis of hyperfine interactions for all materials obtained by using of X-ray powder diffraction (XRPD) and the Rietveld refinement.

The crystalline structure of TlI was firstly investigated at ambient temperature [25]: $Z = 4$, the Pearson symbol oS8, orthorhombic, space group *Cmcm*, $a = 4.57$, $b = 12.92$, $c = 5.24$ Å. In turn, the crystal structure of InI has been determined in [26, 27]: InI, structure type TlI, $Z = 4$, the Pearson symbol oS8, orthorhombic, space group *Cmcm*, $a = 4.763$, $b = 12.781$, $c = 4.909$ Å. *Ab initio* quantum chemistry calculation of the InI compound under high pressure has been performed in Ref. [28]. Up to now many references concerning the investigations of the pseudobinary InI–TlI solid state alloys system are known [16, 17, 21, 24, 29, 30]. Our goal is to study the influence of the cation content change of the samples $In_xTl_{1-x}I$ in the range of $x = 0.0$–0.7, with the increment of 0.1, on the corresponding optical properties.

Also, in the present study, we performed measurements of the photoconductivity spectra for $In_xTl_{1-x}I$ solid state crystalline solutions for the main crystallographic directions, at various contents of Indium x vs. Thallium $1-x$ at ambient temperature $T = 300$ K ($x = 0.5$) and at the temperature of $T = 78$ K ($x = 0.2$, 0.3, 0.4, and 0.5).

3. Experimental

3.1. Crystal growth

Synthesis of the starting material for growing the crystals was realized by the mixing of binary compounds InI and TlI, taken in equimolar ratio [28, 31]. For example, in $In_{0.4}Tl_{0.6}I$ — $m_{Tl} = 11.019$ g, $m_{InI} = 6.560$ g, in $Tl_{0.5}In_{0.5}$ — $m_{Tl} = 15.020$ g, $m_{InI} = 10.930$ g, and in $In_{0.9}Tl_{0.1}I$, $m_{Tl} = 1.011$ g, $m_{InI} = 10.216$ g.

The ampoule of raw was annealed under the pressure 10^{-3} mm Hg in quartz ampoules with the diameter of 12–18 mm, at a temperature above the melting temperature of the high-temperature components, $T_m^{(TlI)} \approx 200$ °C.

Crystal growth was conducted using the vertical Bridgman furnace with the temperature gradient in a furnace equal to 1 K/mm, in quartz ampoules. For the case of $In_{0.4}Tl_{0.6}I$ the growth was realized at the temperature 450 °C. With increase of InI content ($Tl_{0.1}In_{0.9}I$) the temperature was reduced to 430 °C. The ampoules lowering speed of 3 mm/h was here applied during 48 h. After that time, the grown crystals were kept in the same furnace during 24 h at the annealing temperatures being from $T = 190$ °C ($In_{0.4}Tl_{0.6}I$) to $T = 130$ °C ($In_{0.9}Tl_{0.1}I$).

Samples of the grown crystals are presented in Fig. 3. Some samples reached a length of 30–40 mm. All the crystals were quite satisfactory relating a transparency and allow to obtain sections (cuts) of different orientations.

3.2. Structure determination

In order to be sure of the purity and homogeneity of the grown bulk samples, the large single crystals were powdered. XRPD data for X-ray phase analysis and crystal structure refinement were collected in the transmission mode on STOE STADI P diffractometer [32] at the room temperature $T = 295$ K with the following setup: Cu K_{α_1} radiation (X-ray tube voltage $U = 40$ kV, current $I = 35$ mA), curved Ge (111) monochromator on primary beam, $2\theta/\omega$ scan, 2θ angular range for data collection 10.000°−100.225° with the increment of 0.015°, linear position sensitive detector with the 2θ step of recording 0.480° and time per step 100–270 s. A calibration procedure was performed employing NIST SRM 640b (Si) [33] and NIST SRM 676 (Al_2O_3) [34] standards. Analytical indexing of the powder patterns and determination of the space group were performed using N-TREOR09 [35]. The crystal structure was refined by the Rietveld method [36] with the program *FullProf.2k* (version 5.40) [37, 38], applying a pseudo-Voigt profile function and isotropic approximation for the atomic displacement parameters. Absorption correction was accounted by measuring the absorption factor for a sample transmission foil [32] and by Rietveld refinement, according to the type "Transmission geometry (STOE)" [38, 39]. The crystallographic data were standardized with the program STRUCTURE TIDY [39] and the program VESTA [40] was used for structural visualization.

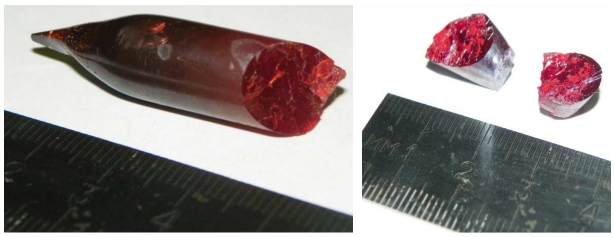

Fig. 3. Typical photo images of studied crystals: (left) $In_{0.5}Tl_{0.5}I$, (right) $In_{0.9}Tl_{0.1}I$.

3.3. Optical absorption and photoconductivity measurements

The coefficient of optical absorption α of the titled crystals as function of the wavelength λ was measured using the fiber optic spectrophotometer AvaSpec-ULS2048-UA-50 (Avantes) in the wavelength range 450–700 nm with 0.5 nm step at the temperature of 78 K. Measurements of absorption spectra were performed at normal incidence of radiation to the crystals surface (001). The thickness of samples studied did not exceed ≈ 1.5 mm.

Photoconductivity spectra (PC) were measured using the monochromator MDR-23 with the spectral resolution of $\Delta\lambda \approx 1$ nm. For measurements at the liquid nitrogen temperature $T = 78$ K, the samples studied were placed into the optical cryostat, which kept temperature stabilised with the accuracy of ± 0.05 K using the temperature regulated cryostat system UTREX. For measurements of photoconductivity in planar samples, the eutectic In–Ga–Sn contacts were attached at the front and back sides of samples [41]. Photoconductivity spectra of $In_xTl_{1-x}I$ were studied at ambient and liquid nitrogen temperatures for different concentrations of indium (x). Measurements were carried out along the c-direction on the ac-surface of the b-cut crystal plate and along the b-direction of the plate.

To clarify the mechanism of PC for the single crystals $In_xTl_{1-x}I$ near the absorption edge spectral region we had recourse to the fact that the spectral dependence of photocurrent generally is consistent with the optical absorption spectrum for thin films. However for thick layers there is a minimum in the photosensitivity spectrum at absorption peak position.

3.4. Method of calculations

The performed calculations were carried out with CASTEP program [42] using the DFT approach. The calculations were realized within the GGA with the PBE exchange-and-correlation functional [43]. The interaction of electrons with the atomic cores was described with the Vanderbilt ultrasoft pseudopotentials [44].

The electronic wave functions are expanded in a plane wave basis set with the energy cut-off of 350 eV. The atomic levels $4d^{10}5s^25p^1$ for In atom, $5d^{10}6s^26p^1$ for Tl atom and $5s^25p^5$ for iodine atom are treated as valence electron states. For the Brillouin-zone sampling, we use the $4 \times 2 \times 2$ Monkhorst–Pack mesh [45]. The self-consistent convergence of the total energy was taken as 5.0×10^{-7} eV/atom. For DFT calculations of $In_xTl_{1-x}I$ solid state solutions the supercells, representing $2 \times 1 \times 1$ unit cells containing 16 atoms, were created. The crystal symmetry of this supercells were reduced to triclinic, $P1$, to remove symmetry operations. The geometry optimization of lattice parameters and internal atomic coordinates were determined using the Broyden–Fletcher–Goldfarb–Shanno (BFGS) minimization technique with the maximum ionic Hellmann–Feynman forces within 0.01 eV/Å, the maximum ionic displacement within 5.0×10^{-4} Å, and the maximum stress within 0.02 GPa. These parameters are sufficiently small to lead to a well-converged total energy of the structures studied.

4. Results and discussion

It was found that the smallest possible content of indium in the grown samples $In_xTl_{1-x}I$ is $x = 0.3$, so that the present study relates to the concentration x in the range of 0.3–1.0 (apart low-temperature structure of TlI). All the investigated samples are single-phase samples, as it was detected by the X-ray diffraction method (XRD). Figure 4 presents a typical XRD pattern for $In_{0.6}Tl_{0.4}I$ sample as example.

A formation of the continuous solid state alloy solution (SSS) between InI and TlI is expected since both components of SSS, InI and low-temperature modification of TlI, are isostructural. Replacement of In atoms by larger Tl ones leads to an increase of the unit cell parameters b and c and to a decrease of the parameter a (Fig. 5, Table I), with a total increase in the volume V of the unit cell. It is interesting to note that the opposite dependences take place for the range 0.4–0.5 of indium concentration x. A decrease of the parameters b and c and an increase of the parameter a, together with decrease of the unit cell volume, could indicate possible structural transformation near the stoichiometric $InTlI_2$ composition.

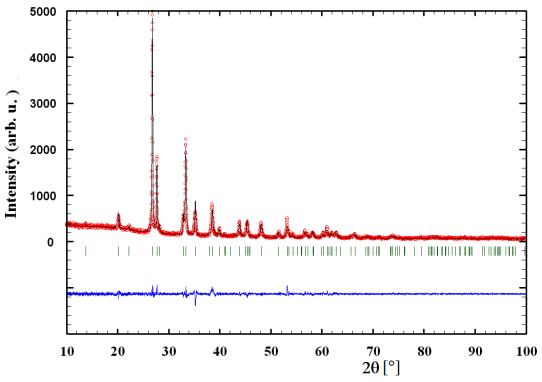

Fig. 4. Measured and calculated XRD patterns for $In_{0.6}Tl_{0.4}I$ (Cu K_{α_1} radiation). Experimental data (circles) and calculated profile (solid line through the circles) are presented together with the calculated Bragg positions (vertical ticks) and difference curve (bottom solid line).

TABLE I

Structural data for $In_xTl_{1-x}I$: space group *Cmcm*, statistical mixture of (In,Tl) atoms and I atoms are positioned in the two Wyckoff positions 4(c) ($0y1/4$). Values of Y, B_{iso} [Å^2] and R_i [%] for In_xTl_{1-x} are given above and for I are below.

x	a	b	c	V	Y	B_{iso}	R_I
	[Å]			[Å^3]		[Å^2]	R_p
1.0	4.7598(2)	12.7649(5)	4.9029(2)	297.90(2)	0.1029(2)	1.6(1)	4.31
					0.35637(19)	0.72(7)	6.13
0.9	4.7496(4)	12.7790(10)	4.9222(4)	298.75(4)	0.10325(19)	1.34(9)	5.01
					0.3566(2)	0.67(7)	8.04
0.8	4.7089(4)	12.8342(9)	5.0088(4)	302.71(4)	0.10335(16)	0.78(8)	4.17
					0.35742(18)	0.91(8)	7.60
0.7	4.6986(4)	12.8511(9)	5.0348(4)	304.01(4)	0.10374(15)	0.68(7)	4.18
					0.35795(18)	1.15(8)	6.71
0.6	4.6671(4)	12.8715(10)	5.0920(5)	305.89(5)	0.10425(15)	0.62(6)	3.95
					0.35868(19)	1.33(9)	6.79
0.5	4.6742(2)	12.8666(6)	5.0775(3)	305.37(3)	0.10405(18)	0.81(7)	4.72
					0.3587(2)	1.0(1)	7.92
0.4	4.6891(4)	12.8643(9)	5.0594(3)	305.19(4)	0.10468(18)	0.7(1)	5.00
					0.3581(2)	1.00(8)	8.21
0.3	4.6600(7)	12.8900(17)	5.1174(8)	307.39(8)	0.1053(2)	0.9(1)	6.51
					0.3591(3)	1.4(1)	8.56

In the crystal structure of this phase, the (In, Tl) and I atoms are connected *via* one bond of the shortest length of ≈ 3.26 Å (Table II). Additionally, each (In, Tl) and I atoms are surrounded by four I and (In, Tl) atoms, respectively (Fig. 6), at four equal distances of ≈ 3.47 Å, thus forming infinite, slightly distorted planar layers.

The photoconductivity spectra of $In_xTl_{1-x}I$ ($x = 0.5$) at room temperature are presented in Fig. 7. Taking into account that the peaks of spectral distribution of photoconductivity are responsible for the phototransitions in the alloy, one can evaluate the band gap energy E_g. It was found to be close to the value $E_g = 2.31$ eV estimated by the absorption band edge of the sample $In_{0.5}Tl_{0.5}I$.

Spectra of PC of the samples studied measured at the liquid nitrogen temperature ($T = 78$ K) are presented in Figs. 8–10. The experimentally observed intense maxima of the PC spectra correspond to the dissociation of the

TABLE II

First coordination inter-atomic distances (smallest and largest) for $In_xTl_{1-x}I$ ($x = 0.3–1.0$).

x	Atoms	Distance [Å]
1.0	I–1In	3.236(4)
	I–4In	3.4560(6)
0.9	I–1(0.9In+0.1Tl)	3.238(4)
	I–4(0.9In+0.1Tl)	3.4583(6)
0.8	I–1(0.8In+0.2Tl)	3.261(3)
	I–4(0.8In+0.2Tl)	3.4740(5)
0.7	I–1(0.7In+0.3Tl)	3.267(3)
	I–4(0.7In+0.3Tl)	3.4783(5)
0.6	I–1(0.6In+0.4Tl)	3.275(3)
	I–4(0.6In+0.4Tl)	3.4864(5)
0.5	I–1(0.5In+0.5Tl)	3.277(3)
	I–4(0.5In+0.5Tl)	3.4839(5)
0.4	I–1(0.4In+0.6Tl)	3.260(4)
	I–4(0.4In+0.6Tl)	3.4822(5)
0.3	I–1(0.3In+0.7Tl)	3.271(5)
	I–4(0.3In+0.7Tl)	3.4909(7)

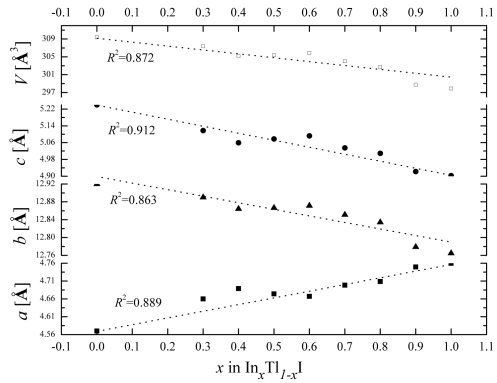

Fig. 5. Unit cell parameters a, b, c, and V as functions of the In content x in the investigated $In_xTl_{1-x}I$ ($x = 0.3–1.0$) samples. The values R^2 are the corresponding coefficients of determination.

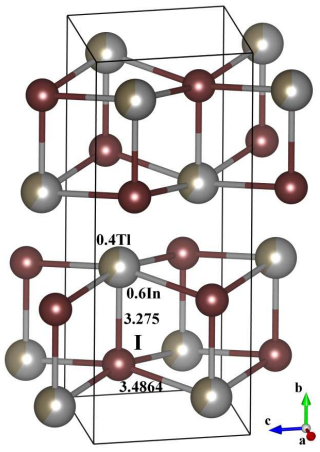

Fig. 6. The crystal structure of $In_xTl_{1-x}I$ ($x = 0.3–1.0$) for $In_{0.6}Tl_{0.4}I$ composition.

electron–hole pairs (excitons). Several mechanisms may cause the exciton dissociation: (a) exciton dissociation with the formation of free electrons and holes that contribute to PC; (b) excitons can recombine due to the photon absorption; (c) exciton dissociation processes based on the longitudinal optical (LO) phonon absorption and emission.

The PC band at 1.2 eV (n-type conductivity) may be attributed to the presence of the photoactive defect centres associated with the anion vacancies or cation interstitials. We suggest that these impurities may cause the electron transitions to the conduction band from the donor levels formed by the cation interstitials, thus being as a source of photoconductivity. These cation defects may form chains along c-direction of the crystal.

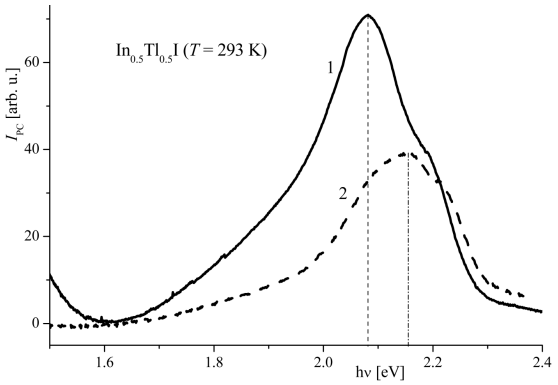

Fig. 7. Photoconductivity spectra of $In_{0.5}Tl_{0.5}$ for the light polarizations $E\|c$ (1) and $E\|b$ (2) at the room temperature $T = 293$ K and the applied voltage $U = 0.1$ V.

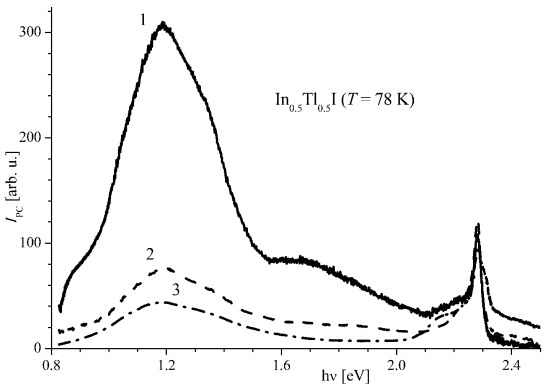

Fig. 8. Photoconductivity spectra of $In_{0.5}Tl_{0.5}$ sample for different light polarizations obtained at the liquid nitrogen temperature ($T = 78$ K): 1 — $E\|c$ (at the applied voltage $U = 9$ V); 2 — $E\|b$ (at the applied voltage $U = 50$ V); 3 — $E\|a$ (at the applied voltage $U = 50$ V).

We observed small anisotropy of the maxima positions in PC spectra obtained at different polarizations for $In_{0.5}Tl_{0.5}$ sample registered in the photon energy range close to the band gap E_g (Table III).

For the case of PC spectrum obtained without applied

TABLE III

Band gap E_g of $In_{0.5}Tl_{0.5}I$ crystal for different orientations of light polarizations E and crystallographic directions a, b, and c obtained from the spectral positions of PC spectra.

Light polarization	$E\|\|a$	$E\|\|b$	$E\|\|c$
E_g [eV]	2.28	2.29	2.28

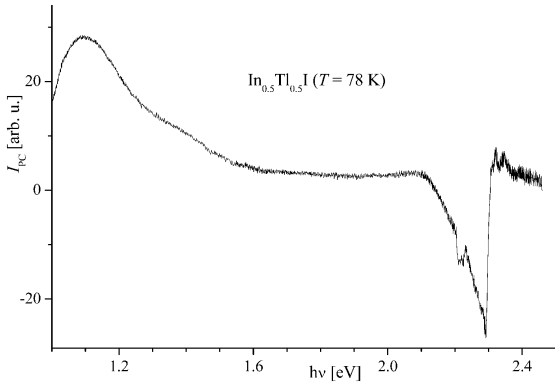

Fig. 9. Photoconductivity spectrum of $In_{0.5}Tl_{0.5}I$ for the polarization $E\|b$ obtained at liquid nitrogen temperature ($T = 78$ K) without applied voltage.

voltage (Fig. 9), a photocurrent observed was of positive and negative signs: the impurity related photoconductivity corresponds to the positive photocurrent and the intrinsic photoconductivity relates to the negative one. The photon energy range of 2.1–2.3 eV, where the photocurrent changes from positive to negative sign, corresponds to the band gap energy E_g. Negative photocurrent of $In_{0.5}Tl_{0.5}I$ in the energy range $h\nu > 2.1$ eV indicates for the predominant p-type of photoconductivity in the material.

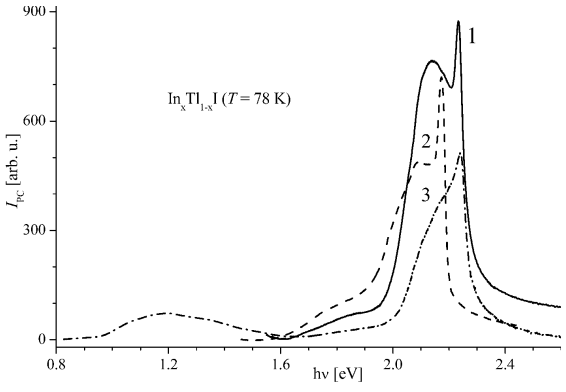

Fig. 10. Photoconductivity spectra of $In_xTl_{1-x}I$ for different contents (1 — $x = 0.7$, 2 — $x = 0.8$, 3 — $x = 0.6$) obtained at the liquid nitrogen temperature ($T = 78$ K) and voltage $U = 50$ V for the light polarization $E\|a$.

In PC spectra of $In_xTl_{1-x}I$ for different values x of indium content (Fig. 10), position of PC peak is spectrally shifted towards higher energies for lower indium contents. For the samples $In_{0.7}Tl_{0.3}I$ and $In_{0.8}Tl_{0.2}I$, the existence of two clear PC peaks in the range 2.1–2.3 eV may be related to the heterogeneity of the samples discussed in Ref. [46]. Another reason that may explain the appearance of two PC spectral peaks in the range 2.1–2.3 eV is a presence of the direct and indirect energy band gaps $E_g^{(d)}$ and $E_g^{(i)}$ of the materials studied [16, 47].

The relatively broad peaks of PC and clear dependence of their spectral positions for different composition of $In_xTl_{1-x}I$ (Figs. 7–10) allow to consider $In_xTl_{1-x}I$ as a promising photosensitive material for the red and near-IR spectral ranges.

Calculations of the band structure of $In_xTl_{1-x}I$ for the index x less than 0.375 seem to be not so interesting because the synthesis and growth of the good quality single crystals for these concentrations are not possible [28]. We have found that SSS $In_{0.3}Tl_{0.7}I$ grown with the indium concentration $x = 0.3$ ($In_{0.3}Tl_{0.7}I$) is polycrystalline.

TABLE IV

Calculated band gap energies E_g of $In_xTl_{1-x}I$ for different x indices of indium content.

x	0.375	0.5	0.625	0.75	0.875	1.0
E_g [eV]	1.718	1.671	1.577	1.539	1.424	1.339

Results of the band structure calculations for InI supercell $2 \times 1 \times 2$ show that direct band gap $E_g^{(d)}$ is not placed at the high symmetry point Q of the BZ (as mentioned in Ref. [17]), but at between Γ and Z points. This fact points to the inaccuracy of the InI and $In_xTl_{1-x}I$ band energy spectra in Ref. [17].

The measurements of the absorption spectra (Fig. 11) were performed in order to check the theoretically calculated parameter E_g with experimental data. The theoretical results are in a good agreement with experimental data.

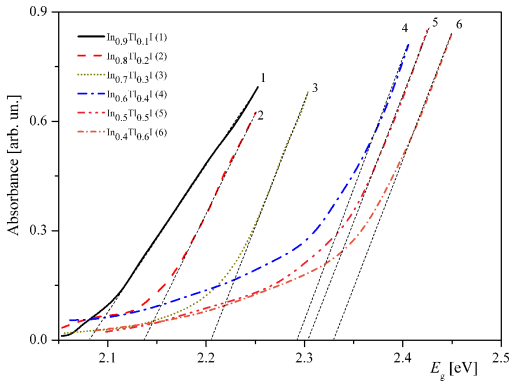

Fig. 11. Absorption spectra of $In_xTl_{1-x}I$ ($x = 0.4-0.9$) at liquid nitrogen temperature ($T = 78$ K).

A decreasing character of the band gap dependences on the indium content $E_g(x)$ was found for the experiment (Fig. 11) and *ab initio* calculations (Fig. 12). In both cases however, clear deviations from straight lines of the same character are observed (Fig. 12). The principle

TABLE V

Energies of band gap E_g of $In_xTl_{1-x}I$ for different x indices of indium content obtained from optical absorption measurements at the temperature $T = 78$ K.

x	0	0.4	0.5	0.6	0.7	0.8	0.9	1.0
E_g [eV]	2.84	2.33	2.31	2.29	2.21	2.14	2.08	2.01 [46]

explanation for this seem to be the Burstein–Moss effect [48], which is caused by the excess carriers (electrons and holes) of the doping atoms. These excess carriers lead to the increase of the band gap E_g.

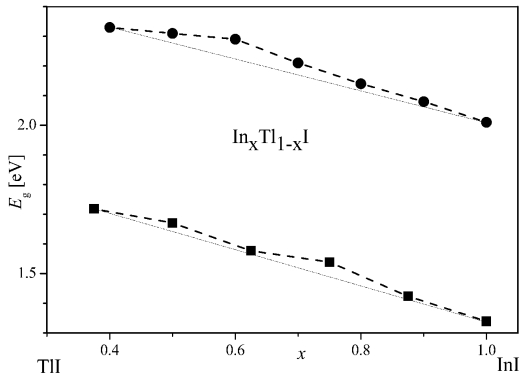

Fig. 12. Concentration dependences of the band gap $E_g(x)$ of $In_xTl_{1-x}I$ determined from absorption spectra (circles) and from *ab initio* calculations (squares).

Additionally, for all crystalline alloys studied, one can see a clear difference of anisotropy between the valence and conduction band dispersions $E(K)$. The top of valence band is more flat and the conduction band shows higher dispersion. It is caused by the fact that the holes have less mobility with respect to the electrons. The top of the valence band is formed prevailingly by p-anionic (iodine) and s-cationic (indium and thallium) states and the bottom of the conduction band is formed by p-cationic states. The substitution of thallium by indium leads to the increase of the effective masses of the particular holes and electrons, that is seen from the analysis of the dispersion $E(K)$ in Fig. 13. This behavior is evidently caused by the known inverse dependence of the dispersion $E(K)$ (and corresponding inverse effective mass $\mathrm{d}^2E/\mathrm{d}K^2$) and the crystal unit cell volume V_c (for the materials studied, $In_xTl_{1-x}I$, the inverse relation between V_c and x takes place). Maximal dispersion $E(K)$ is observed for the bands in the direction $\Gamma-F-Q$ and $\Gamma-Z$ of BZ, when the critical points corresponding to the band gap E_g are taken place at $\Gamma-Z$ segment of the BZ.

5. Conclusions

The chemical synthesis and crystal growth of the solid state alloys $In_xTl_{1-x}I$ have been realized in the whole possible range of the indium content $x = 0.375-1.0$ and the X-ray based crystal structure of these materials have been studied. On the basis of the crystal structures obtained, the optical and photoconductivity spectra of

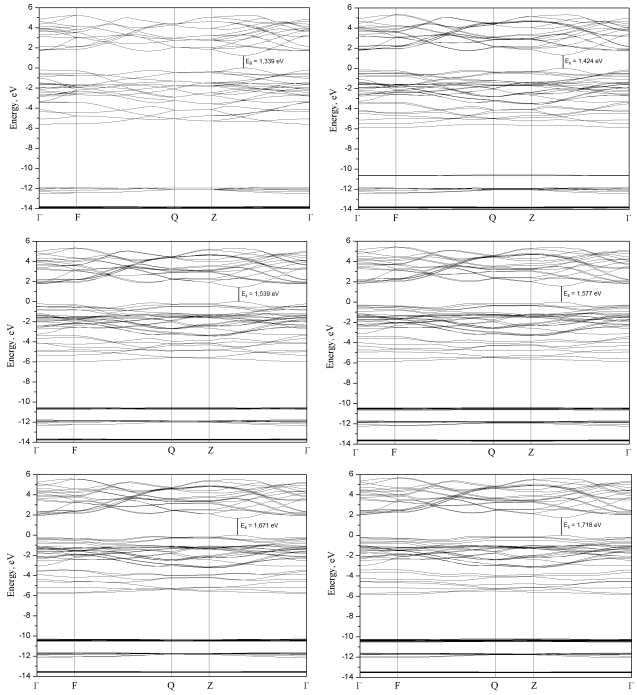

Fig. 13. Electronic band structures (dispersions) $E(K)$ of $In_xTl_{1-x}I$ for $x = \begin{matrix} 1 & 0.625 \\ 0.875 & 0.5 \\ 0.75 & 0.375 \end{matrix}$.

$In_xTl_{1-x}I$ were studied for the first time both experimentally and theoretically. Good correlation between the experimental (optically defined from absorption spectra) and calculated band gap energies E_g for $In_{1-x}Tl_xI$ solid state alloys have been detected. A decreasing character of the band gap dependences on the indium content $E_g(x)$ was found from the experimental and theoretical DFT-based studies.

The impurity related photoconductivity found in $In_{1-x}Tl_xI$ crystals has been attributed to the n-type conductivity caused by donor levels and formed by the cation interstitials arranged along the crystallographic c-axis direction.

Acknowledgments

Calculations have been performed using the Materials Studio package at the supercomputer center of Wrocław University of Technology (WCSS), Poland.

References

[1] P. Bhattacharya, M. Groza, Y. Cui, D. Caudel, T. Wrenn, A. Nwankwo, A. Burger, G. Slack, A.G. Ostrogorsky, *J. Cryst. Growth* **312**, 1228 (2010).

[2] I. Nicoara, D. Nicoara, C. Bertorello, G.A. Slack, A.G. Ostrogorsky, M. Groza, A. Burger, *MRS Proc.* **1341**, mrss11-1341-u09-01 (2011).

[3] F. Dybała, M.P. Polak, J. Kopaczek, P. Scharoch, K. Wu, S. Tongay, R. Kudrawiec, *Sci. Rep.* 6, 26663 (2016).

[4] R. Browning, P. Plachinda, P. Padigi, R. Solanki, S. Rouvimov, *Nanoscale* **8**, 2143 (2016).

[5] I.V. Kityk, M.I. Kolinko, A.V. Franiv, *Ferroelectrics* **130**, 347 (1992).

[6] M.I. Kolinko, I.V. Kityk, A.S. Krochuk, *J. Phys. Chem. Solids* **53**, 1315 (1992).

[7] Ya.O. Dovgii, I.V. Kityk, M.I. Kolinko, A.S. Krochuk, A.V. Franiv, M.K. Zamorskii, *Phys. Status Solidi B* **167**, 637 (1991).

[8] I. Kolinko, A.S. Krotschuk, I.V. Kityk, *Phys. Status Solidi B* **134**, K83 (1992).

[9] M.I. Kolinko, I.V. Kityk, A.B. Kozhljuk, *Acta Phys. Pol. A* **84**, 1065 (1993).

[10] M.I. Kolinko, *J. Phys. Condens. Matter* **6**, 183 (1994).

[11] Z. Wei, X. Zhao-Peng, W. Hai-Yan, C. Fei-Hong, H. Chang, *Acta Phys. Sin.* **62**, 243101 (2013).

[12] M.I. Kolinko, R.Y. Bibikov, *Zeits. Phys. B Condens. Matter* **95**, 167 (1994).

[13] M.I. Kolinko, *Phys. Rev. B* **B55**, 4007 (1997).

[14] M.I. Kolinko, A.H. Nevidomskyy, *J. Phys. Stud.* **4**, 437 (2000).

[15] M.I. Kolinko, O.V. Bovgyra, *Ukr. J. Phys.* **46**, 707 (2001).

[16] A. Franiv, O. Bovgyra, O. Savchyn, *Ukr. J. Phys.* **51**, 269 (2006).

[17] X. Zhao-Peng, W. Yong-Zhen, Z. Wei, W. Qian, W. Guo-Qing, *Acta Phys. Sin.* **63**, 147102 (2014).

[18] M. Yoshida, N. Ohno, K. Nakamura, Y. Nakai, *J. Phys. Soc. Jpn.* **52**, 1108 (1983).

[19] K.S. Shah, J.C. Lund, F. Olschner, J. Zhang, L.P. Moy, M.R. Squillante, W.W. Moses, S.E. Derenzo, *IEEE Trans. Nucl. Sci.* **41**, 2715 (1994).

[20] A.V. Churilov, G. Ciampi, H. Kim, W.M. Higgins, L.J. Cirignano, F. Olschner, V. Biteman, M. Minchello, K.S. Shah, *J. Cryst. Growth* **312**, 1221 (2010).

[21] Ya.O. Dovgyi, S.V. Ternavska, A.V. Franiv, *Ukr. J. Phys.* **47**, 61 (2002).

[22] I.V. Blonskyy, A. Krochuk, T.L. Stetsyshyn, A.V. Franiv, *Sov. Phys. Solid State* **28**, 3136 (1986).

[23] N. Ohno, K. Nakamura, Y. Nakai, *J. Phys. Soc. Jpn.* **56**, 2565 (1987).

[24] A.V. Franiv, *Herald Lviv. Univ. Phys. Series* **30**, 92 (1998).

[25] L. Helmholz, *Z. Kristallogr.* **95**, 129 (1936).

[26] R.E. Jones, D.H. Templeton, *Acta Crystallogr.* **8**, 847 (1955).

[27] G. Meyer, T. Staffel, *Z. Anorg. Allg. Chem.* **574**, 114 (1989).

[28] D. Becker, H.P. Beck, *Z. Kristallogr.* **219**, 348 (2004).

[29] A.I. Kashuba, A.V. Franiv, O.V. Bovgyra, R.S. Brezvin, *Funct. Mater.* **24**, 26 (2017).

[30] A.I. Kashuba, S.V. Apunevych, *J. Nano-Electron. Phys.* **8**, 01010 (2016).

[31] V.G. Korshunova, *Phases Equilibrium in Halogenic Systems*, Metallurgy, Moscow 1979, p. 180.

[32] STOE & Cie GmbH, WinXPOW 3.03, *Powder Diffraction Software Package*, Darmstadt, Germany 2010.

[33] SRM 640b: Silicon Powder $2\theta/d$-Spacing Standard for X-ray Diffraction, National Institute of Standards and Technology, U.S. Department of Commerce, Gaithersburg (MD) 1987.

[34] SRM 676: Alumina Internal Standard for Quantitative Analysis by X-ray Powder Diffraction, National Institute of Standards and Technology, U.S. Department of Commerce, Gaithersburg (MD) 2005.

[35] A. Altomare, G. Campi, C. Cuocci, L. Eriksson, C. Giacovazzo, A. Moliterni, R. Rizzi, P.-E. Werner, *J. Appl. Crystallogr.* **42**, 768 (2009).

[36] *The Rietveld Method, IUCr Monographs on Crystallography*, Vol. 5, Ed. R.A. Young, Oxford University Press, New York 1993, p. 298.

[37] J. Rodriguez-Carvajal, *Commission on Powder Diffraction (IUCr), Newsletter* **26**, 12 (2001).

[38] T. Roisnel, J. Rodriguez-Carvajal, *Mater. Sci. Forum* **378-381**, 118 (2001).

[39] L.M. Gelato, E. Parthé, *J. Appl. Crystallogr.* **20**, 139 (1987).

[40] K. Momma, F. Izumi, *J. Appl. Crystallogr.* **44**, 1272 (2011).

[41] R.V. Gamernyk, Y.P. Gnatenko, A.G. Slivka, *J. Phys. Stud.* **12**, 4703 (2008).

[42] S.J. Clark, M.D. Segall, C.J. Pickard, P.J. Hasnip, M.J. Probert, K. Refson, M.C. Payne, *Zeits. Kristallogr.* **220**, 567 (2005).

[43] J.P. Perdew, K. Burke, M. Ernzerhof, *Phys. Rev. Lett.* **77**, 3865 (1996); J.P. Perdew, K. Burke, M. Ernzerhof, *Phys. Rev. Lett.* **78**, 1396 (1997).

[44] D. Vanderbilt, *Phys. Rev.* **B41**, 7892 (1990).

[45] H.J. Monkhorst, J.D. Pack, *Phys. Rev.* **B13**, 5188 (1976).

[46] C.A. Gaw, C.R. Kannewurf, *Appl. Phys. Lett.* **38**, 634 (1981).

[47] I.V. Kityk, M.I. Kolinko, A. Krochuk, A. Franiv, *Sov. Phys. Solid State* **33**, 225 (1991).

[48] M. Grundmann, *The Physics of Semiconductors*, Springer-Verlag, Berlin 2006.